Full Paper

Journal of the Brazilian Chemical Society

https://dx.doi.org/10.21577/0103-5053.20250186

J. Braz. Chem. Soc. **2026**, *37*, e-20250186, 1-12

Thermal Decomposition Kinetics of Corticosteroids Prednisone, Betamethasone Valerate and Hydrocortisone Acetate by Applying a MLP Network

Daniel F. Pessoa,[a] *Maria Betânia F. Marques,*[a,b] *Wagner N. Mussel*[a] *and Rita C. O. Sebastião*[*,b]

[a]*Departamento de Química, Instituto de Ciências Exatas (ICEx), Universidade Federal de Minas Gerais (UFMG), Av. Pres. Antônio Carlos, 6627, Pampulha, 31270-901 Belo Horizonte-MG, Brazil*

[b]*Faculdade de Ciências Farmacêuticas (FCF), Universidade Federal de Alfenas (UNIFAL-MG), Rua Gabriel Monteiro da Silva, 700, Centro, 37130-001 Alfenas-MG, Brazil*

Corticosteroids are widely prescribed to treat inflammatory conditions. Understanding their thermal stability is essential to ensure their safety and efficacy during storage, processing, and pharmaceutical use. This study investigated the non-isothermal decomposition kinetics of prednisone, betamethasone valerate, and hydrocortisone acetate using thermogravimetric analysis. Vyazovkin Isoconversional Method was employed to evaluate the activation energy profiles, followed by kinetic model fitting to determine the pre-exponential factors. A multilayer perceptron neural network was implemented to identify the most suitable reaction mechanisms and complete the kinetic triplet for the reaction. Thermal analysis revealed three decomposition events for prednisone and betamethasone valerate and two events for hydrocortisone acetate, reflecting the influence of structural differences on their stability. The neural network provided more accurate predictions than the single kinetic models and indicated that most decomposition steps followed the Avrami-Erofeev model. In this context, nucleation and growth are interpreted as the stochastic initiation and propagation of reactive nuclei through molecular rearrangements and diffusion in the amorphous or liquid phases, rather than crystallization phenomena. Although originally developed for isothermal conditions, the Avrami-Erofeev approach has been widely and successfully applied to dynamic heating experiments as a phenomenological model for describing decomposition kinetics. These results provide unprecedented insights into corticosteroid stability, contributing to preformulation, quality control, and pharmaceutical development.

Keywords: corticosteroids, non-isothermal kinetics, Vyazovkin Isoconversional Method, multilayer perceptron network

Introduction

Corticosteroids were discovered in the 1940s and are used to treat various types of inflammation and autoimmune diseases,[1-3] such as dermatological, ophthalmological, rheumatological, hematological, pulmonary and gastrointestinal disorders.[1,2] One of their main applications is in asthma treatment, administered via inhalation, but they can also be used to treat several other allergic problems.[4]

The term corticosteroid is used to describe agents with glucocorticoid activity, such as cortisol, a natural hormone produced by the adrenal glands, which interferes with glucose metabolism.[5] Prednisone (Figure 1a), betamethasone valerate (Figure 1b) and hydrocortisone acetate (Figure 1c) are some widely used synthetic examples.[6-11]

In addition to traditional uses, these drugs have recently been applied in the coronavirus disease 2019 (COVID-19) pandemic to treat severe cases of this disease, being able to reduce mortality and the need for mechanical ventilation in hospitalized patients.[12-16]

Thus, it is important to know the physicochemical characteristics of these active pharmaceutical ingredients (API) to understand their behavior in drug products and biopharmaceutical properties and to elucidate the variables that affect their stability. In this way, several studies have already been carried out to identify and quantify, or to study the pharmacokinetics,

*e-mail: ritacos@ufmg.br
Editor handled this article: Adriana Nunes Correia (Associate)

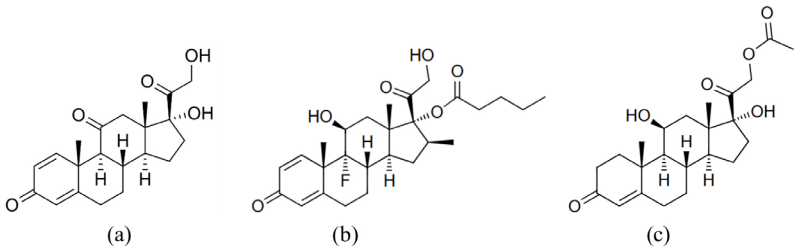

Figure 1. Graphical representation of the molecular structures of the corticosteroids: (a) prednisone, (b) betamethasone valerate, and (c) hydrocortisone acetate.

pharmacodynamics and their use as therapy in the fight against various comorbidities.[3,5,17-23] Some studies focused on evaluating the stability of these corticoids,[24-32] but few addresses their thermal behavior and decomposition kinetics in the solid state.[26,33]

Consequently, further studies are needed to elucidate the stability and and thermal decomposition kinetics of these APIs, especially for corticoids commonly applied in drug formulations. Thereby, this study aims to investigate the stability and kinetics of three widely used corticosteroids: prednisone, betamethasone valerate and hydrocortisone acetate which, from this point on, will be designated respectively as PSONE, BSONE and HSONE. To perform this study, samples were analyzed using thermogravimetry (TG/DTG/DTA), differential scanning calorimetry (DSC), and X-ray diffraction (XRD). The Vyazovkin Isoconversional Method was then applied to calculate the activation energies (E_a), and kinetic models were used to obtain the pre-exponential factor (A) from the experimental data of TG curves. Finally, a Multilayer Perceptron Network (MLP) was used to elucidate the kinetic mechanisms of the thermal decomposition of corticoids.

As temperature is a critical process parameter (CPP) within Good Manufacturing Practices (GMP) for drug products, knowledge of the thermal properties of corticosteroids and the kinetic parameters related to thermal stability are very useful for pharmaceutical manufacturing.[34,35]

Experimental

Materials and reagents

The samples API raw material were: prednisone 97.96% (batch 23B10-B009-101266; tolerance limit 97-102%) obtained from China, betamethasone valerate 101.37% (batch 23A17-B024-100267; tolerance limit 97-103%) obtained from India, and hydrocortisone acetate 99.5% (batch 20230207; tolerance limit 97-103%) obtained from China, all with content within the acceptance limit established by the United States Pharmacopeia (USP-22).[36]

Instrumentation

Simultaneous thermogravimetry (TG)/differential thermal analysis (DTA) was conducted using a Shimadzu DTG-60H instrument in a dynamic N_2 atmosphere at a flow of 50.0 mL min^{-1}. Experiments were carried out from room temperature up to 600.0 °C, with heating rates of 10.0, 15.0, and 20.0 °C min^{-1} for PSONE and BSONE. The HSONE rates were 2.0, 6.0, and 10.0 °C min^{-1}. These heating rates were selected because they provided three non-overlapping curves suitable for kinetic calculations. The samples were accurately weighed to approximately 2.5 mg in an open alumina crucible. The TG curves were differentiated in the 1st order (DTG) to confirm the temperature range of the observed phenomena. A differential scanning calorimetry (DSC) 60 plus Shimadzu cell was used under a dynamic N_2 atmosphere with a flow of 50 mL min^{-1} and heating rate of 10 °C min^{-1} in the range of 30-400 °C. A closed aluminum crucible and sample mass of 2.0 mg, accurately weighed, were used for analysis. The equipment was previously calibrated with indium (T_{onset} = 156.63 °C, melting enthalpy (ΔHm) = 28.45 J g^{-1}).

X-ray diffraction (XRD) was performed using an Anton Paar XRDynamic 500 diffractometer at 40 KV and 50 mA, using a NiCu monochromator with a Cu tube, 1D detector, and steel 25 mm sample holder without an internal standard. The setup conditions were 4-50° 2θ, step size of 0.02° 2θ, with 15 s of acquisition time, with peak position calibrated with LaB_6.

Kinetic methods

The investigation was conducted using the obtained TG curves (see the "Instrumentation" sub-section). To perform the kinetic calculations, the Vyazoykin isoconversional method was applied to obtain the activation energies, and 15 different $f(\alpha)$ models (see Table 1) were used to calculate the pre-exponential factor, both E_a and A as a function of α (conversion degree). To complete the study, a non-isothermal MLP neural network was used to investigate the mechanisms involved in the thermal decomposition of corticosteroids. Calculations were performed using MATLAB software[37] with custom codes.

Table 1. The fifteen kinetic models used in the MLP network to model corticoids thermal decomposition kinetics

	Kinetic model	f(α)	g(α)
1	First-order (F1)	$1-\alpha$	$-\ln(1-\alpha)$
2	Second-order (F2)	$(1-\alpha)^2$	$(1-\alpha)^{-1}-1$
3	Avrami-Erofeev (Am2)	$2(1-\alpha)[-\ln(1-\alpha)]^{1/2}$	$[-\ln(1-\alpha)]^{1/2}$
4	Avrami-Erofeev (Am3)	$3(1-\alpha)[-\ln(1-\alpha)]^{2/3}$	$[-\ln(1-\alpha)]^{1/3}$
5	Avrami-Erofeev (Am4)	$4(1-\alpha)[-\ln(1-\alpha)]^{3/4}$	$[-\ln(1-\alpha)]^{1/4}$
6	Avrami-Erofeev (Am15)	$3/2((1-\alpha)[-\ln(1-\alpha)]^{1/3}$	$[-\ln(1-\alpha)]^{2/3}$
7	Avrami-Erofeev (Am25)	$5/2((1-\alpha)[-\ln(1-\alpha)]^{3/5}$	$[-\ln(1-\alpha)]^{2/5}$
8	Prout-Tompkins (Au)	$\alpha/1-\alpha$	$\ln(\alpha/(1-\alpha))$
9	Linear contraction (R1)	1	α
10	Contracting area (R2)	$2(1-\alpha)^{1/2}$	$1-(1-\alpha)^{1/2}$
11	Contracting volume (R3)	$3(1-\alpha)^{2/3}$	$1-(1-\alpha)^{1/3}$
12	1-D Diffusion (D1)	$1/(2\alpha)$	α^2
13	2-D Diffusion (D2)	$-[1/\ln(1-\alpha)]$	$((1-\alpha)\ln(1-\alpha))+\alpha$
14	3-D Diffusion-Jander (D3)	$3(1-\alpha)^{2/3}]/[1-(1-\alpha)^{1/3}]$	$(1-(1-\alpha)^{1/3})^2$
15	Ginstling- Brounshtein (D4)	$3/[2((1-\alpha)^{-1/3}-1)]$	$1-(2/3)\alpha-(1-\alpha)^{2/3}$

f(α): reaction mechanism; g(α): reaction mechanism in integral form; α: conversion degree.

Vyazovkin Isoconversional Method

The Vyazovkin Isoconversional Method[38] was employed to determine the activation energy for the thermal decomposition of corticoids. The fundamental kinetic equation,[39] $\frac{d\alpha}{dt}=k(T)\times f(\alpha)$ can be used to describe the rate of thermal decomposition of a solid sample, where $\alpha=\frac{m_t-m_0}{m_f-m_0}$ is the reaction conversion degree, with m_0 being the initial mass, m_f the final mass and m_t the mass at time t.

Assuming the Arrhenius equation for the rate constant of the process, $k(T)=A\exp\left(\frac{-E_a}{RT}\right)$, where A, R and E_a are the pre-exponential factor, the universal gas constant, and activation energy, respectively. Under non-isothermal conditions with constant heating rates, $\left(\beta=\frac{dT}{dt}\right)$, the decomposition rate $\left(\frac{d\alpha}{dt}\right)$ can be rewritten as $\left(\beta\frac{d\alpha}{dT}\right)$. Therefore, the fundamental kinetic equation for these processes is as follows:

$$\beta\frac{d\alpha}{dT}=A\exp\left(\frac{-E_a}{RT}\right)\times f(\alpha) \quad (1)$$

where the function f(α) is the reaction mechanism, which can be obtained by assuming different kinetic models (Table 1).

Rearranging and integrating equation 1, the following expression is obtained:

$$g(\alpha)=\frac{A}{\beta}\int\exp\left(\frac{-E_a}{RT}\right)dT=\frac{A}{\beta}I(E,T) \quad (2)$$

with $g(\alpha)=\int\frac{d\alpha}{f(\alpha)}$ and $I(E,T)=\int\exp\left(\frac{-E_a}{RT}\right)dT$.

Integral of equation 2, I(E,T), does not have an analytical solution. Therefore, it can be calculated using some approximation functions available in the literature,[40,41] or obtained numerically (the method used in this work) for more accurate results. Assuming that the reaction model is independent of the heating rate (β), equation 2 can be rearranged as follows (equation 3).

$$\frac{A_\alpha}{\beta_1}I(E_\alpha,T_{\alpha1})=\ldots=\frac{A_\alpha}{\beta_n}I(E_\alpha,T_{\alpha n}) \quad (3)$$

with the subindex n indicating different heating rates. According to the Vyazovkin Isoconversional Method, the activation energy of the process can be obtained for different α values by determining E_a that minimizes equation 4. In addition, the pre-exponential factor can be calculated for each kinetic model (Table 1) using the obtained E_a values.

$$\sum_{i=1}^{n}\sum_{j\neq i}^{n}\frac{I(E_\alpha,T_{\alpha,i})\beta_j}{I(E_\alpha,T_{\alpha,j})\beta_i}=\min \quad (4)$$

Multilayer Perceptron Network (MLP)

To study the thermal decomposition kinetics of corticosteroids, a Multilayer Perceptron (MLP) was employed to treat the non-isothermal data obtained through TG analysis. Thus, a network comprising three layers (input, output, and hidden) was used. The architecture of the proposed MLP is shown in Figure 2.

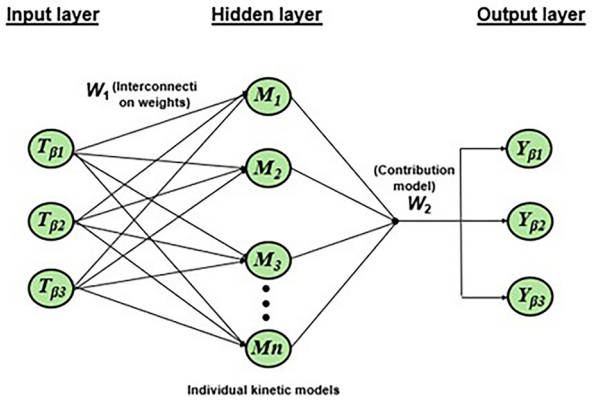

Figure 2. MLP neural network architecture to investigate the thermal decomposition kinetics of corticoids.

The temperatures at different reaction conversion degrees for each heating rate (β_i) were provided to the neurons in the input layer. At least three neurons are necessary according to the International Confederation for Thermal Analysis and Calorimetry (ICTAC) protocol.[42] Each neuron corresponds to a distinct heating rate dataset. Interconnection weights ($\mathbf{W_1}$) between the intermediate and input layers can be obtained using an approximation function or calculated numerically to maximize precision.

Neurons in the intermediate layer represent specific kinetic models activated by $g(\alpha)$. The matrix $\mathbf{B_n} = g(W_1(T_{\alpha i}))$, consisting of m experimental data and p kinetic models, is constructed for each heating rate. Considering n heating rates, optimization of the following multi-objective function, MOF, is required:

$$\mathrm{MOF} = \left(\mathbf{W_2B_1} - \mathbf{Y_1}\right)^2 + \left(\mathbf{W_2B_2} - \mathbf{Y_2}\right)^2 + \ldots + \left(\mathbf{W_2B_n} - \mathbf{Y_n}\right)^2 \quad (5)$$

where $\mathbf{W_2}$ is the vector of interconnection weights between the intermediate and output layers, and $\mathbf{Y_n}$ is the experimental $\alpha(T)$ data at the heating rate β_i.

Matrices with high conditions indicate an ill-posed problem; therefore, a well-established Tikhonov regularization method[43,44] was used to solve equation 5. The optimization of $\mathbf{W_2}$ can be described as the contribution of each kinetic model used here, providing a physical meaning for a process that cannot be adequately explained by an individual model.

The performance of the MLP architecture was evaluated using mean squared errors (MSEs), as shown in equation 6, by comparing the individual model results with those of the proposed MLP architecture.

$$\mathrm{MSE} = \frac{1}{m}\sum_{j=1}^{m}\left(y_{exp.j} - y_{calc.j}\right)^2 \quad (6)$$

Here, m is the total number of points, $y_{exp.j}$ the experimental data and $y_{calc.i}$ the predicted data.

Results and Discussion

Thermal behavior

To evaluate the effects of temperature on corticosteroid stability, DSC and TG/DTA curves were obtained at 10 °C min^{-1} (Figure 3). The temperature range of the observed phenomena was confirmed by DTG (pink line). PSONE melted at T_{onset} 228.36 °C with an enthalpy of 101.7 J g^{-1}. BSONE melted at T_{onset} 185.6 °C with an enthalpy change of 57.28 J g^{-1}. HSONE melted at T_{onset} 218.75 °C with an enthalpy of 117.17 J g^{-1}. The three corticosteroids have high thermal stabilities (> 195 °C).

Before the melting event, the DSC curves of the three corticosteroids presented an endothermic phenomenon at ca. 100 °C, with a small amount of heat involved (< 1 J g^{-1}) and without mass loss (confirmed by TG curves), as shown in the enlarged view in Figure 3. The residue separation after the phenomenon at ca. 105 °C, with cooling of the sample and subsequent thermal and XRD analyses, showed that the structures did not change in relation to the source material, maintaining the same phenomenon, melting, and XRD pattern. Therefore, this endothermic phenomenon at ca. 100 °C may be related to the chain rearrangement characteristics of the steroid nucleus (a structure common to all corticosteroids). The amount of heat involved and the results of the XRD investigation confirm that this is a rearrangement in the steroid nucleus, where the only observation is the change in the number of diffractor centers in the concerned plane without mass loss. As expected, the only reflection on the diffractogram was a small change in the peak intensities owing to a higher or lower number of electrons diffracting the electromagnetic radiation. No crystalline lattice transition to another lattice was observed, the space group remained unaltered, the lattice parameters were the same, the peaks still centered at the same angle, and the symmetry relationships remained the same. The only observed differences were the slight variations in peak intensities. This is characteristic of small changes in the plane occupation and, therefore, changes in the observed peak intensities of the related planes.

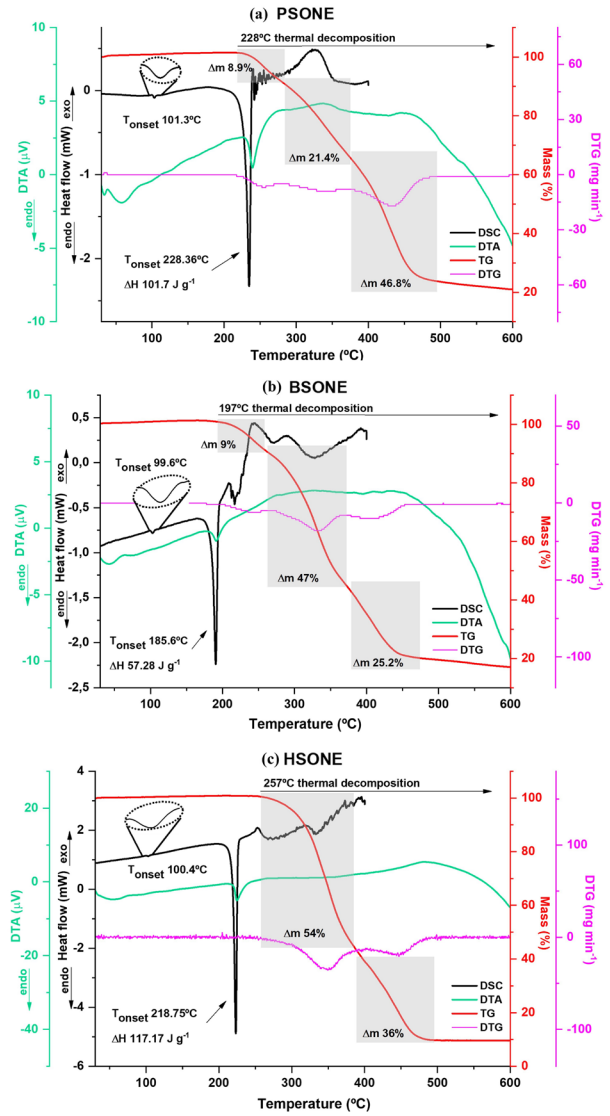

Figure 3. Thermal behaviors of corticosteroid drugs: (a) prednisone (PSONE); (b) betamethasone valerate (BSONE); and (c) hydrocortisone acetate (HSONE) as determined by differential scanning calorimetry (black line), differential thermal analysis (green line), thermogravimetry (red line), and derivative thermogravimetry (pink line).

The thermal properties of test drugs are critical material attributes (CMA) that must be considered when defining the manufacturing conditions. The temperature reached in a unit operation, for example, through heat dissipation, can induce phase transitions that compromise the biopharmaceutical performance of the product. Therefore, kinetic studies of thermal processes provide detailed information about the behavior of molecules, as described in this study.

TGA and $\alpha \times T$ curves for the corticoids PSONE, BSONE and HSONE are shown in Figure 4, as a standard procedure, the events were normalized (0 to 1), with $\frac{d\alpha}{dt} \times T$ plottings on Figure 5. Three events were observed for PSONE and BSONE and two for HSONE, in accordance with the DTG curves shown in Figure 3. The temperatures and mass loss of decomposition for each event were as follows: for PSONE, 220-320 °C, Δm 8.9% in the 1st event (PSONE-1); 320-387 °C, Δm 21.4% in the 2nd event (PSONE-2); and 387-500 °C, Δm 46.8% in the 3rd event (PSONE-3); for BSONE: 220-289 °C, Δm 7.9% (BSONE-1); 289-396 °C, Δm 47% (BSONE-2); and 396-500 °C, Δm 25.2% (BSONE-3); and for HSONE, from 200 to 380 °C, Δm 54% (HSONE-1) and 380 to 500 °C, Δm 36% (HSONE-2).

Several pharmaceutical ingredients are subject to inter and intramolecular interactions, such as hydrogen bonding and steric repulsions, which are generally promoted by group sizes. Molecules with higher inter- and/or intra-hydrogen bonding interactions require high energy for melting, lattice movements, defect corrections, and direct melting and/or melting immediately followed by decomposition, when not directly decomposing. Corticoid molecules have a similar basic structure that undergoes such responses to heat. However, they exhibit different interaction energies.

The lattice energy can be correlated with the sublimation enthalpy by considering the electronic relaxation energy associated with the transition from the crystal to the gas phase, as well as the difference in vibrational energies between the two phases. This relationship can be reasonably approximated, since it is important to note that crystals where minimal molecular geometry change occurs between the crystal and gas phases, the sublimation enthalpy is a positive quantity, with its magnitude at room temperature being approximately 5 kJ mol^{-1} less than that of the lattice energy. Conformational polymorphism is prevalent in API because of their significant internal flexibility. Any attempt to estimate the relative stability of polymorphs must also account for the energy differences between the various conformations present in the polymorphs.[45]

The interaction energies were determined using CrystalExplorer Open Computacional Chemistry project, by Peter R Spacman, Perth, Australia V25.09 Model Energies, 2025,[45] which are characterized by four primary components: electrostatic, polarization, dispersion, and exchange-repulsion energies. To achieve precise values for the electrostatic, polarization, and repulsion energies, monomer wavefunctions at the HF/3-21G, MP2/6-31G(d,p), and B3LYP/6-31G(d,p) levels were used, supplemented by Grimme's D2 dispersion corrections. Three energy models originally developed by fitting dispersion-corrected density functional theory (DFT) energies for numerous pairs of neutral molecules derived from organic (and some inorganic) molecular crystals were employed. The most effective model from the initial study replicated B3LYP-D2/6-31G(d,p) counterpoise-corrected energies with a mean absolute deviation (MAD) slightly

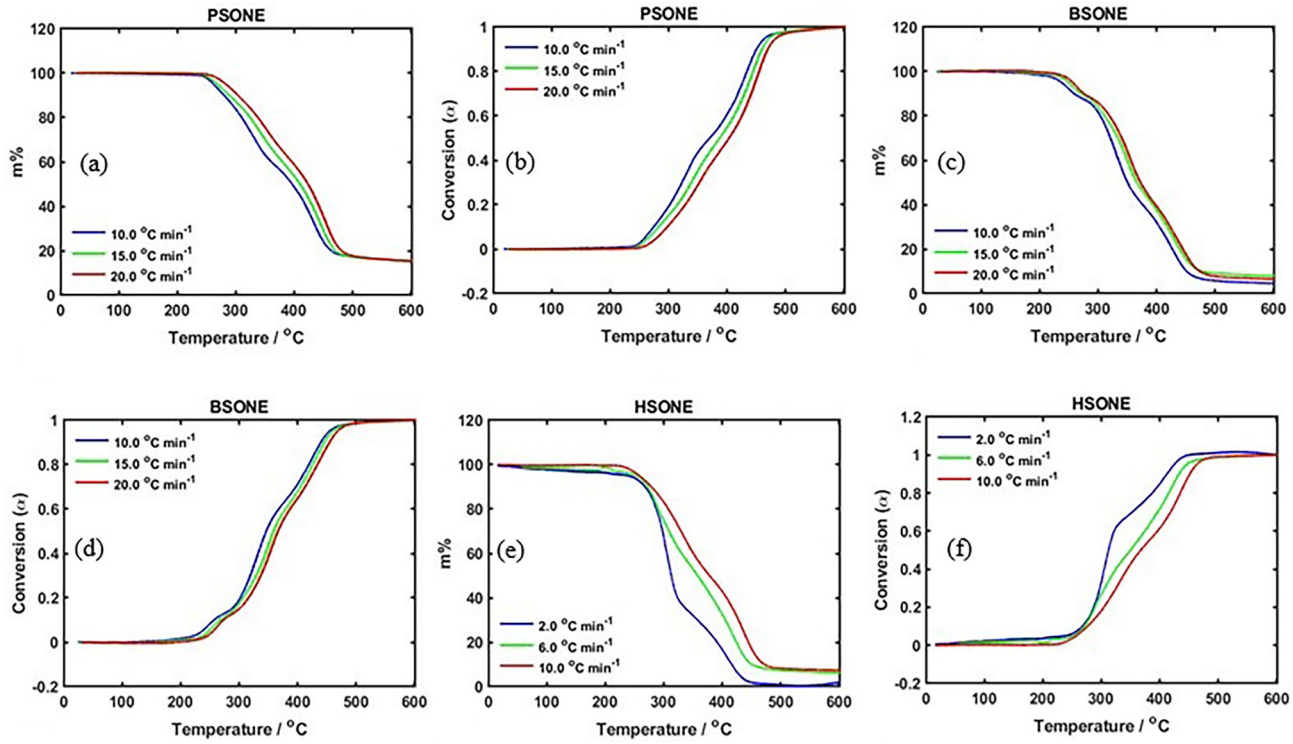

Figure 4. TGA experimental data and normalized conversion degree α in function of temperature. (a,b) prednisone (PSONE); (c,d) betamethasone valerate (BSONE); and (e,f) hydrocortisone acetate (HSONE).

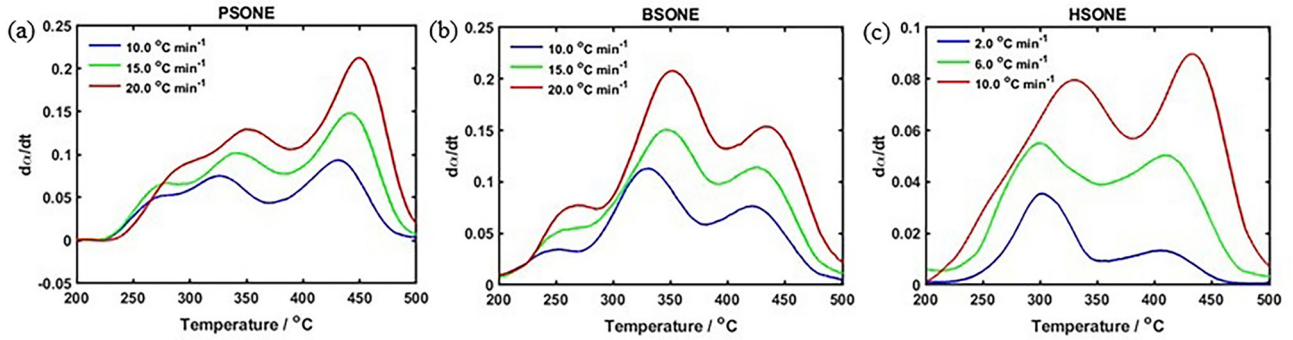

Figure 5. Calculated $\frac{d\alpha}{dt} \times T$ for the corticosteroids (a) prednisone (PSONE); (b) betamethasone valerate (BSONE); and (c) hydrocortisone acetate (HSONE).

exceeding 1 kJ mol^{-1} while requiring significantly less computational time. These models evaluate the interaction energy of two molecules within a unit cell.[45]

Prednisone presented −1178 Eh, betamethasone valerate presented −3388 Eh and hydrocortisone acetate presented −1331 Eh, where Eh is the energy in Hartree units, corresponding to 1 Eh to 27.211 electron-volts (eV) or 4.359×10^{-18} joules (J). Therefore, even with a basic similar molecular structure, the interaction energies are different, inducing exchanges in the interactions under heat.

For the observed phenomena that have no mass loss in the TG curves, the only reasonable explanation, since there is no loss or gain in reflection planes under X-ray diffraction experiments, is the existence of small movements and dislocations in the molecules comprising the asymmetric unit. Small enough to have the energies observed in the heat experiment, which leads to few angle exchanges in certain planes and results in an increase or decrease in the diffractor centers on that plane, generating only intensity changes on the already observed reflections on the diffractograms, as expected by the presence of a higher or lower number of electrons on the considered plane. These movements did not characterize polymorph interconversions, as the geometric descriptions were still the same for the same special group, with symmetric relationships all over the diffractor centers and point symmetry.

X-ray diffraction also confirmed the pure samples of all corticosteroids used in the present study: PSONE, BSONE, and HSONE, as can be visualized in the XRD diffractograms (Figure 6). The experimental patterns

indicate pure starting materials with no contribution from any crystalline phase of order for all the corticoid samples.

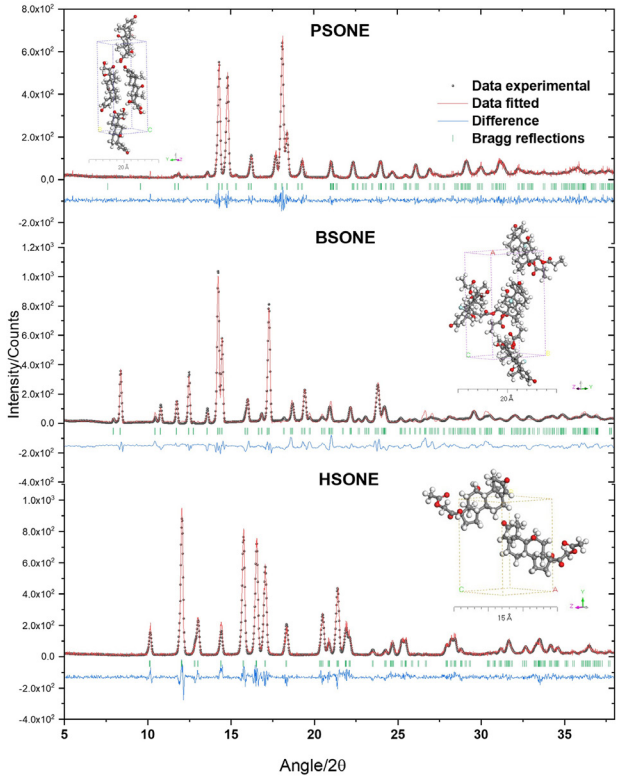

Figure 6. Rietveld-fitted patterns for prednisone (PSONE); betamethasone valerate (BSONE); and hydrocortisone acetate (HSONE).

Activation energies and pre-exponential factors

The thermal decomposition curves indicated that the processes occurred through more than one event, that is, a multi-step mechanism; therefore, they were separated and studied independently. For each process, the activation energy (E_a) was calculated using the Vyazovkin Isoconversional Method, and the values obtained are displayed in Figure 7. In addition, the pre-exponential factors were calculated for each kinetic model, as listed in Table 1. The obtained E_a and logA values are listed in Table 2, where the pre-exponential factors are displayed for the main kinetic model, as evidenced by the MLP.

The onset temperature of thermal decomposition occurs at 197 °C for BSONE, 228 °C for PSONE, and 257 °C for HSONE. Although the order of the initial decomposition temperature is BSONE < PSONE < HSONE, the average activation energy of the first event does not follow this same trend.

The onset temperature values are used to compare the relative thermal stability of the corticosteroids, as is commonly done in thermal analysis. However, it is important to note that the onset temperature of a decomposition process cannot be inferred solely from the activation energy, it is obtained through an analysis of the kinetic triplet: E_a, A, and reaction mechanism, $f(\alpha)$.

The activation energy is expressed as a function of conversion, $E_a(\alpha)$, allowing the identification of possible changes in the reaction mechanism throughout the thermal decomposition. We can note that in all events analyzed, A has the same behavior of E_a, which states these parameters follow the kinetic compensation effect.

The dependence of the kinetic triplet to explain the onset temperature can be performed by considering equation 1, which rearranged, can be obtained:

$$\frac{\beta}{Af(\alpha)}\frac{d\alpha}{dT} = \exp\left(\frac{-E_a}{RT}\right) \quad \text{and,}$$

$$T = -\frac{E_a}{R\log\left(\frac{\beta}{Af(\alpha)}\frac{d\alpha}{dT}\right)} \tag{7}$$

A lower onset temperature does not necessarily imply a lower activation energy (or average E_a value). A higher onset

Table 2. Calculated E_a and logA for the thermal decomposition of corticosteroids

α	PSONE-1		PSONE-2		PSONE-3		BSONE-1		BSONE-2		BSONE-3		HSONE-1		HSONE-2	
	E_a / (kJ mol^{-1})	logA	E_a / (kJ mol^{-1})	logA	E_a / (kJ mol^{-1})	logA	E_a / (kJ mol^{-1})	logA	E_a / (kJ mol^{-1})	logA	E_a / (kJ mol^{-1})	logA	E_a / (kJ mol^{-1})	logA	E_a / (kJ mol^{-1})	logA
0.1	70.6	10.4	84.1	12.7	182.3	28.1	68.9	10.8	142.6	24.8	176.3	26.6	368.9	76.1	95.6	9.6
0.2	63.4	8.7	86.0	12.7	164.8	24.3	74.6	12.2	126.7	21.0	185.2	27.8	385.3	77.0	112.5	12.6
0.3	59.6	7.9	86.4	12.5	168.6	24.6	84.1	14.5	113.1	17.9	193.8	29.1	209	37.3	127.4	15.2
0.4	56.2	7.1	87.9	12.7	166.9	24	87.6	15.3	105.5	16.1	195.2	29.1	163.6	27.1	142.8	17.8
0.5	54.2	6.6	87.5	12.4	165.5	23.5	89.9	15.9	101.6	15.2	196.3	29.1	149.1	23.6	158.1	20.4
0.6	54.2	6.6	88.0	12.4	167.8	23.7	91.5	16.2	102.7	15.2	194.5	28.6	131.2	19.7	171.5	22.7
0.7	53.7	6.5	86.2	11.9	170.6	24.0	91.9	16.3	104.9	15.5	197.3	28.8	113	15.7	184.4	24.8
0.8	54.2	6.6	89.6	12.5	179.4	25.2	87.3	15.2	104.2	15.2	200.2	29.1	91.6	11.2	191.2	25.8
0.9	54.1	6.7	100.7	14.5	201.5	28.7	83.8	14.4	109.4	15.9	220.2	32.2	74.7	7.7	196.6	26.4

α :reaction conversion degree; E_a: activation energy; A: pre-exponential factor (in s^{-1}); PSONE-1: prednisone event 1; PSONE-2: prednisone event 2; PSONE-3: prednisone event 3; BSONE-1: betamethasone valerate event 1; BSONE-2: betamethasone valerate event 2; BSONE-3: betamethasone valerate event 3; HSONE-1: hydrocortisone acetate event 1; HSONE-2: hydrocortisone acetate event 2.

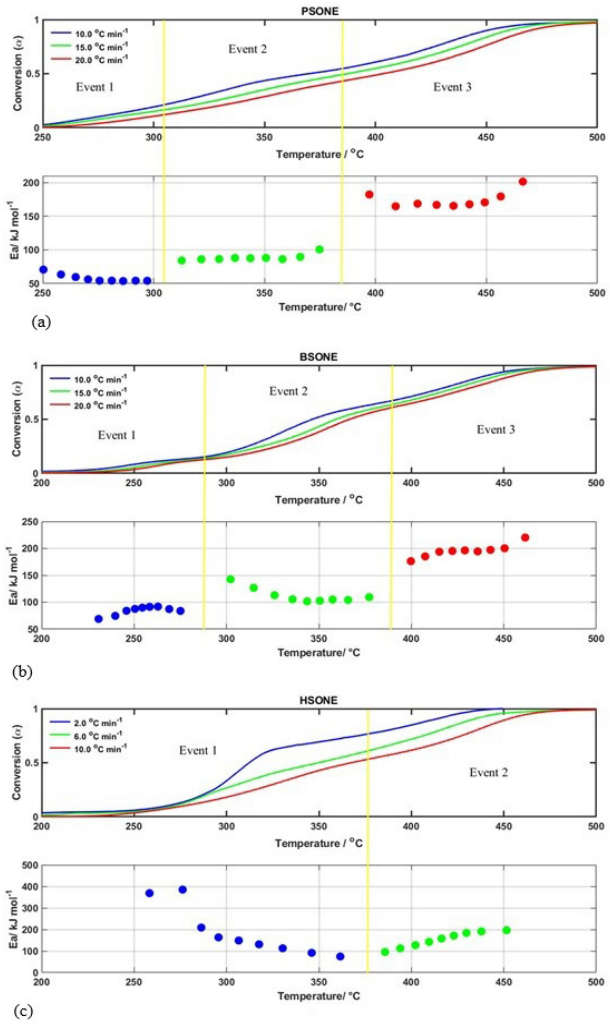

Figure 7. Activation energy along the thermal decomposition process for (a) prednisone (PSONE); (b) betamethasone valerate (BSONE); and (c) hydrocortisone acetate (HSONE).

temperature can be obtained even if E_a (or average E_a) is lower, as long as A, f(α) or a combination of these parameters compensates the E_a value. The initial temperatures of the decomposition process were calculated for the first event to the three corticoids considering α = 10%, activation energy at this conversion degree, frequency factor and only one kinetic model (the model that showed the greatest contribution from the neural network). The frequency factor was determined from equations 2 and 3 considering this same kinetic model. The calculated temperature presented a residual error of 2.6% for BSONE, 3.3% for PSONE and 7.9% for HSONE validating the determined kinetic triplet and highlighting the process must be described as a combination of kinetic models, once the adjustment of the MLP (considering this combination of kinetic models) presented much smaller residual error, with the same E_a and A.

From the calculated data, it can be seen that prednisone first event (PSONE-1) presented a decrease in E_a and A until α = 0.4, followed by a stabilization of these kinetic parameters for the rest of the event. The maximum E_a obtained was 70.6 kJ mol^{-1}, and the minimum was 53.7 kJ mol^{-1}, with an average value of 57.8 kJ mol^{-1}. Prednisone second event (PSONE-2) exhibited a slight growth trend, with a maximum E_a of 100.7 kJ mol^{-1}, a minimum of 84.1 kJ mol^{-1}, and an average value of 88.5 kJ mol^{-1}. Comparing the E_a result for the 2nd event with the results of Ledeti *et al.*,[33] the average E_a calculated here (88.5 kJ mol^{-1}) is close to that obtained by the integral isoconversional methods used in that study. However, these values deviate significantly when compared to the Friedman differential technique[46-48] calculated in that work, which could indicate undervalued values for the latter, since the Vyazovkin Isoconversional Method holds high accuracy when performed with numerical integration.[42,49,50] For prednisone third event (PSONE-3), we first have a decrease in E_a, then an increasing behavior after α = 0.5. The maximum, minimum, and average E_a were 201.5, 164.8, and 174.2 kJ mol^{-1}, respectively. The pre-exponential factor exhibited the same trend as the activation energy for this step. These results suggest that during the thermal decomposition process, PSONE yields a stable conformational intermediate, as more energy is required to complete the decomposition. For example, in the first event, there was a mass loss of 8.9%, which corresponds to 31.9 g mol^{-1}. This result can be attributed to the –CH_2OH group as the initial leaving group. This suggestion is corroborated by the average E_a determined as about 50 kJ mol^{-1} and total (sum) of 520 kJ mol^{-1} for the first step, which is consistent with the breaking of one carbon-carbon bond (ca. 350 kJ mol^{-1}) with some energy required to break intermolecular interactions. Thus, one can suggest, from the combination of these results, that the thermal decomposition process must start with the –CH_2OH group leaving the corticosteroid nucleus. After this group leaves the molecule, the residual corticosteroid nucleus can possibly rearrange with more effective intermolecular and/or intramolecular interactions, yielding a more stable intermediate. This discussion is a suggestion to be evaluated, as it is necessary to perform XRD analysis of the intermediates. These analyses will be performed in future studies.

Betamethasone first event (BSONE-1) exhibited crescent E_a values, with a small decrease after α = 70%. The maximum, minimum, and average activation energies were 91.9, 68.9, and 84.4 kJ mol^{-1}, respectively. For betamethasone second event (BSONE-2), E_a maximum was 142.6 kJ mol^{-1}, minimum of 101.6, and 112.3 kJ mol^{-1} for the average. Betamethasone third event (BSONE-3) displayed E_a values of 220.2 kJ mol^{-1} for the maximum value, 176.3, and 195.4 kJ mol^{-1} as the maximum, minimum, and average values, respectively. For all the BSONE events, the

pre-exponential factors displayed the same tendency as the activation energies, i.e., following the kinetic compensation effect. Similar to PSONE, the average E_a increased from the previous to the next step of thermal decomposition, indicating the formation of more stable species along the thermal decomposition process. For BSONE, the activation energy also increased along the decomposition process, suggesting the stabilization of intermediates by inter- or intramolecular interactions. The first BSONE event shows a mass loss of approximately 9%, which is consistent with a mass loss of approximately ca. 43 g mol^{-1}. In this case, the suggested groups leaving are $-CH_2OH$ and $-CH_3$. The average and total (sum) E_a values for this first event corroborate this suggestion, as it is approximately 84 and 760 kJ mol^{-1} respectively, which corresponds to two carbon-carbon bond breaking and some energy required for weakening intermolecular interactions. Similar to the PSONE, this discussion is also a suggestion for evaluation. A complete analysis will be performed in future studies.

Hydrocortisone acetate first event (HSONE-1) maximum, minimum, and average calculated activation energies were respectively: 385.3, 74.7 and 187.4 kJ mol^{-1}, respectively. The hydrocortisone acetate second event (HSONE-2) activation energies increased, with a small decrease after α = 80%. was 196.6, of 95.6, and 153.3 kJ mol^{-1} for for the average. The pre-exponential factor exhibited a behavior similar to that of E_a in both HSONE events. Unlike the other corticoids investigated, the average E_a decreased when the next step was reached; therefore, we can conclude that the decomposition products are less stable than hydrocortisone acetate. The average activation energy for the initial 30% of HSONE thermal decomposition was superior to 200 kJ mol^{-1}, with total of 1686 kJ mol^{-1} for the first event, the mass loss was approximately 54% or 218.4 g mol^{-1}. This combined analysis suggests that the HSONE molecule possibly decomposes with the breaking of many structural bonds. By comparing the molecular structures of these corticoids, one can suggest that the thermal decomposition of PSONE and BSONE starts with the smaller leaving groups, $-CH_2OH$ and $-CH_3$ (BSONE only). In contrast, this process is not the same for HSONE, which presents an expressive mass loss for the first event. The processes started with a higher activation energy and decreased along the process, indicating that the decomposition intermediates were not stabilized by inter- or intramolecular interactions.

Kinetic mechanisms of corticosteroids thermal decomposition

The thermal decomposition mechanisms obtained using the MLP network are illustrated in Figure 8. For PSONE-1, PSONE-2, HSONE-1, HSONE-2, and BSONE-2, Am2 (Avrami-Erofeev order n = 2) was the main reaction model, whereas Am25 (Avrami-Erofeev order n = 2.5) was the principal model for the other reactions. Other differences were observed in the model distribution of drug thermal decomposition. Nevertheless, all events resulted in a combination of Avrami-Erofeev models[51-54] for all corticoid events, as shown in Figure 8. This is evidence that the nucleation and growth (with diffusion) mechanisms are the limiting steps for the reactions to proceed.

The Avrami-Erofeev kinetic equation, which originally describes the formation of a new phase along the thermal decomposition process, can also be applied in a broader interpretation, for example, to model stochastic initiation of active reaction sites inside the material. The subsequent growth process of the nuclei represents the propagation of these reaction fronts through diffusion and molecular rearrangements in the liquid or amorphous phase.[55,56]

Therefore, when the kinetic analysis indicates an Avrami-Erofeev-type mechanism, it suggests that the limiting step of decomposition is associated with the initiation and spatial propagation of reactive centers rather than crystallization phenomena. This broader interpretation of nucleation and growth has been widely adopted in the thermal decomposition studies of amorphous or liquid systems.

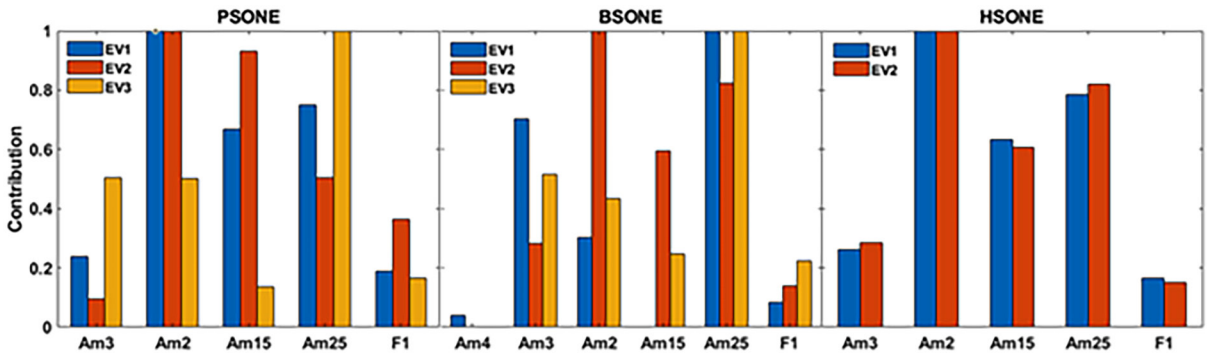

Figure 8. Normalized contribution of kinetic models in the MLP result to describe corticosteroid thermal decomposition events, with EV1 as Event 1, EV2 as event 2 and EV3 as event 3.

The Avrami-Erofeev model was originally formulated for isothermal transformations. Nevertheless, its use under non-isothermal conditions has been widely reported in thermal decomposition studies, particularly for organic and pharmaceutical compounds, where it often provides a satisfactory description of the experimental data.

For example, the Avrami-Erofeev function has been successfully applied to the nonisothermal decomposition of amitriptyline,[57] biomass,[58] and pyrolysis of phosphate tailings,[59] among other systems, all studied under linear heating programs. In these cases, the model served not as a rigorous isothermal derivation but as a phenomenological function capable of capturing nucleation-and-growth-type kinetics even in the absence of crystalline nuclei.

We fully acknowledge the theoretical limitations associated with applying Avrami's equation outside isothermal conditions, as emphasized in the literature.[60] However, under well-controlled heating rates, this approach has been considered a reasonable approximation to describe the overall kinetics of thermal decomposition, and our use of the model was based on its ability to best fit the experimental data compared with alternative mechanistic functions.

From Figure 9, we can observe that the proposed MLP showed a good fit with the conversion curves calculated from the experimental data for the PSONE events. This was confirmed by the network error compared to the conversion values from the TG data, which was below 10^{-11} for the three steps, indicating the quality of the MLP in reproducing the experimental curves, together with the validation of the calculated activation energy and frequency factor.

The applied MLP was also able to successfully describe the BSONE thermal decomposition events, as shown in Figure 10, where the circles (obtained by the MLP mechanism and activation energy and frequency factor determined) were adequately adjusted to the conversion curves of experimental data.

Similar to the PSONE events, the calculated errors between the network and experimental data were below 10^{-11} for the BSONE processes, corroborating the high-quality of the proposed MLP.

Finally, the MLP was adequate for modeling the HSONE thermal degradation steps, as shown in Figure 11, where the circles indicate the values obtained by the network and the curves are the calculated conversions from the experimental data. The calculated error of the MLP compared to the experimental values was below 10^{-7} for the two thermal decomposition events. This confirms the quality of the MLP applied to corticosteroids and also validates the activation energy and frequency factor determined for all studied corticoids.

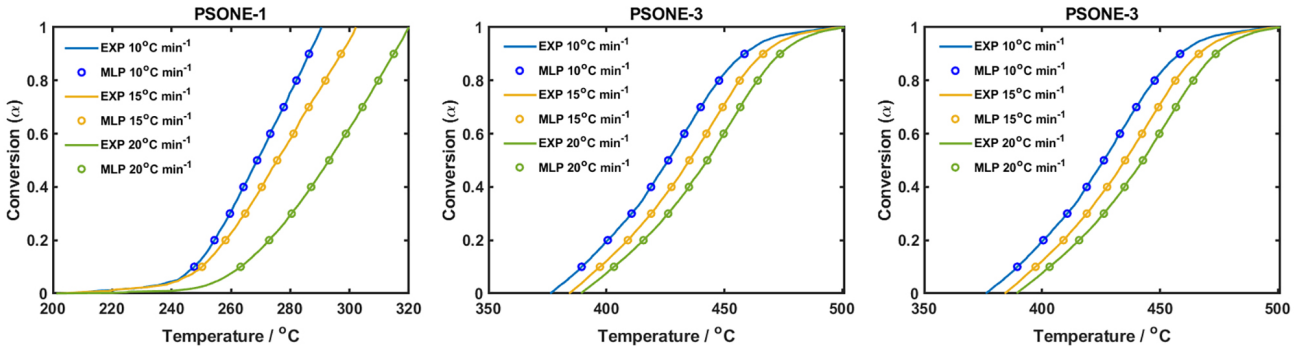

Figure 9. MLP values (in circles) plotted above the conversion curves for (a) PSONE-1, (b) PSONE-2, and (c) PSONE-3. P-EV for PSONE (prednisone) events 1, 2 or 3.

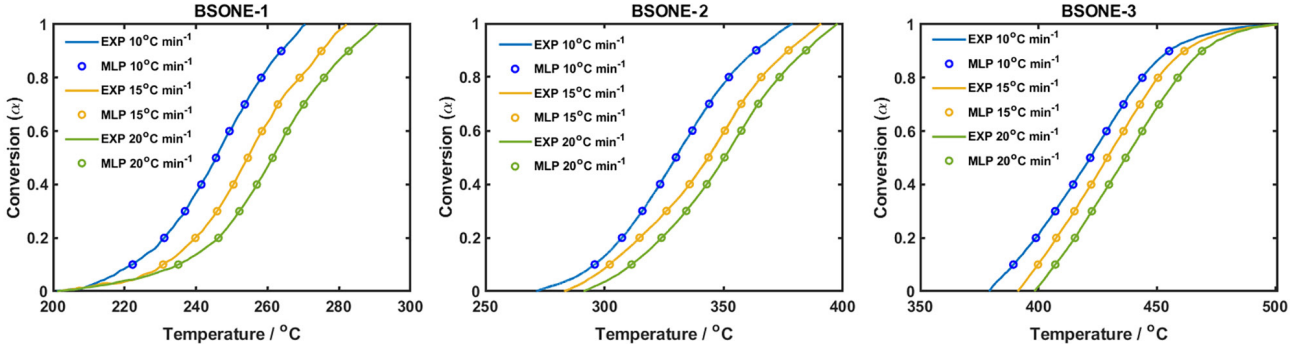

Figure 10. MLP values (in circles) plotted above the conversion curves for (a) BSONE-1, (b) BSONE-2, and (c) BSONE-3. BSONE (betamethasone valerate) events 1, 2 or 3.

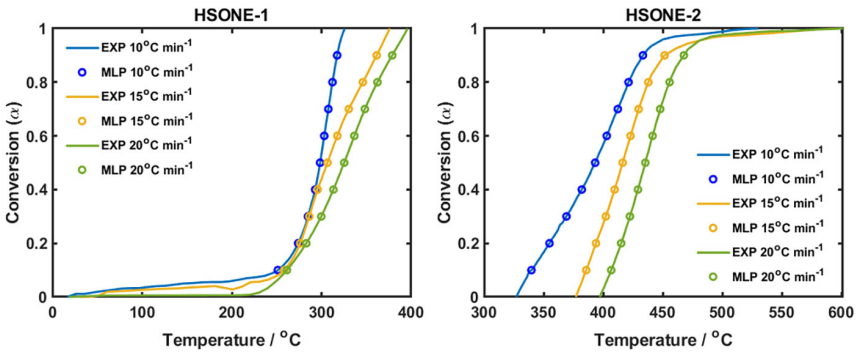

Figure 11. MLP values (in circles) plotted above the conversion curves for (a) HSONE-1 and (b) HSONE-2. HSONE (hydrocortisone acetate) events 1 and 2.

Conclusions

In this study, we successfully investigated the thermal behavior, including the decomposition kinetics, of three widely prescribed corticosteroids, PSONE, BSONE, and HSONE, using a non-isothermal approach. Thermogravimetric analyses revealed multi-step decomposition mechanisms: three distinct events for PSONE and BSONE and two for HSONE.

The E_a and A varied throughout the conversion process, indicating complex and temperature-dependent degradation pathways during the conversion process. Notably, PSONE and BSONE displayed an increase in E_a in the later decomposition steps, suggesting the formation of more stable intermediates, whereas HSONE exhibited the opposite trend.

The MLP neural network was effective in modelling the thermal decomposition behavior of all corticosteroids. It outperformed the individual kinetic models in fitting the experimental data and revealed that the thermal decomposition mechanisms predominantly followed the Avrami-Erofeev models, indicating nucleation and growth processes.

Overall, this study highlights the relevance of kinetic modelling in understanding API stability and demonstrates the potential of neural networks as powerful tools for kinetic analysis.

Data Availability Statement

All data are available in the text.

Acknowledgments

This study was financed in part by CAPES (Finance Code 001). The authors also thank CNPq (305870/2023-8), FAPEMIG for financial support and Amphora compounding pharmacy for sample donation.

Author Contributions

D.F.P. was responsible for formal analysis, writing original draft; M.B.F.-M. for conceptualization, data curation, formal analysis, investigation, methodology, validation, visualization, writing original draft; W.N.M. for data curation, investigation, methodology, writing original draft; R.C.O.S. for project administration, investigation, methodology, formal analysis, roles, and writing original draft.

References

1. Liu, D.; Ahmet, A.; Ward, L.; Krishnamoorthy, P.; Mandelcorn, E. D.; Leigh, R.; Brown, J. P.; Cohen, A.; Kim, H.; *Allergy, Asthma, Clin. Immunol.* **2013**, *9*, 30. [Crossref]
2. Hodgens, A.; Sharman, T.; *Corticosteroids*; StatPearls: Treasure Island, USA, 2023. [Link] accessed in December 2025
3. Möhlmann, J. E.; Ezzafzafi, S.; Lindemans, C. A.; Jansen, M. H. A.; Nierkens, S.; Huitema, A. D. R.; Luin, M. V.; *Clin. Pharmacokinet.* **2024**, *63*, 1251. [Crossref]
4. Barnes, P. J.; *Eur. J. Pharmacol.* **2006**, *533*, 2. [Crossref]
5. Williams, D. M.; *Respir. Care* **2018**, *63*, 655. [Crossref]
6. Vis, R.; Mathijssen, H.; Keijsers, R.G. M.; van de Garde, E. M.W.; Veltkamp, M.; Akdim, F.; Post, M. C.; Grutters, J. C.; *J. Nucl. Cardiol.* **2023**, *30*, 1543. [Crossref]
7. Mizerska-Wasiak, M.; Starczyński, M.; Wasiak, W.; Małdyk, J.; Płatos, E.; Pańczyk-Tomaszewska, M.; *J. Clin. Med.* **2024**, *13*, 7316. [Crossref]
8. Barajas-Mendoza, I.; Castillo-Rodríguez, I. O.; Hernández-Rioja, I.; Ramirez-Apan, T.; Martínez-García, M. M.; *Steroids* **2024**, *205*, 109395. [Crossref]
9. Gether, L.; Linares, H. P. I.; Kezic, S.; Jakasa, I.; Forman, J.; Sørensen, O. E.; Storgaard, H.; Skov, L.; Røpke, M. A.; Knop, F. K.; Thyssen, J. P.; *J. Eur. Acad. Dermatol. Venereol.* **2025**, *39*, 308. [Crossref]
10. Tawfik, Y. M.; Hofny, E. R. M.; Zidan, F. M.; Ghazally, A.; *Arch. Dermatol. Res.* **2025**, *317*, 342. [Crossref]
11. Pinarbasli, O.; Atilgan, N.; Turkes, E.; Sarracoglu, N.; Doganay, A. A.; *Pharmaceutics* **2025**, *17*, 348. [Crossref]
12. Paassen, J. V.; Vos, J. S.; Hoekstra, E. M.; Neumann, K. M. I.; Boot, P. C.; Arbous, S. M.; *Crit. Care* **2020**, *24*, 696. [Crossref]
13. Chaudhuri, D.; Sasaki, K.; Karkar, A.; Sharif, S.; Lewis, K.; Mammen, M. J.; Alexander, P.; Ye, Z.; Lozano, L. E. C.;

Munch, M. W.; Perner, A.; Du, B.; Mbuagbaw, L.; Alhazzani, W.; Pastores, S. M.; Marshall, J.; Lamontagne, F.; Annane, D.; Meduri, G. U.; Rochwerg, B.; *Intensive Care Med.* **2021**, *47*, 521. [Crossref]
14. Romano, G. M.; Cafiero, T.; Frangiosa, A.; Robertis, E.; *Minerva Anestesiol.* **2021**, *87*, 1042. [Crossref]
15. Johns, M.; George, S.; Taburyanskaya, M.; Poon, Y. K.; *J. Pharm. Pract.* **2022**, *35*, 626. [Crossref]
16. Kuo, W. T.; Lai, I. H.; *Glob. Chall.* **2025**, e00223. [Crossref]
17. Kuperminc, E.; Heming, N.; Carlos, M.; Annane, D.; *J. Clin. Med.* **2023**, *12*, 3340. [Crossref]
18. Chen, Y.; Li, K.; Pu, H.; Wu, T.; *Cochrane Database Syst. Rev.* **2011**, CD007720. [Crossref]
19. Belanoff, J. K.; Gross, K.; Yager, A.; Schatzberg, A. F.; *J. Psychiatr. Res*. **2001**, *35*, 127. [Crossref]
20. Annane, D.; Bellissant, E.; Bollaert, P. E.; Briegel, J.; Keh, D.; Kupfer, Y.; *Cochrane Database Syst. Rev*. **2015**, *2015*, CD002243. [Crossref]
21. Esposito, M. C.; Santos, A. L. A.; Bonfilio, R.; de Araújo, M. B.; *Crit. Rev. Anal. Chem.* **2020**, *50*, 111. [Crossref]
22. Frerichs, V. A.; Tornatore, K. M.; *J. Chromatogr. B: Anal. Technol. Biomed. Life Sci.* **2004**, *802*, 329. [Crossref]
23. Pujos, E.; Flament-Waton, M. M.; Paisse, O.; Grenier-Loustalot, M. F.; *Anal. Bioanal. Chem*. **2005**, *381*, 244. [Crossref]
24. Hansen, J.; Bundgaard, H.; *Int. J. Pharm.* **1980**, *6*, 307. [Crossref]
25. de Medeiros, A. C. D.; de Cervantes, N. A. B.; Gomes, A. P. B.; Macêdo, R. O.; *J. Therm. Anal. Calorim.* **2001**, *64*, 745. [Crossref]
26. Khattak, S. U.; Sheikh, D.; Ahmad, I.; Usmanghani, K.; *Indian J. Pharm. Sci.* **2012**, *74*, 133. [Crossref]
27. Romão, J. S.; Hamdy, M. S.; Mul, G.; Baltrusaitis, J.; *J. Hazard. Mater.* **2015**, *282*, 208. [Crossref]
28. Cacciari, R. D.; Reynoso, E.; Montejano, H. A.; Biasutti, M. A.; *Photochem. Photobiol. Sci.* **2017**, *16*, 1717. [Crossref]
29. Guo, Z.; Guo, A.; Guo, Q.; Rui, M.; Zhao, Y.; Zhang, H.; Zhu, S.; *Chem. Eng. J.* **2017**, *307*, 722. [Crossref]
30. Jahani, M.; Akaberi, M.; Heidari, T.; Kamali, H.; Nejabat, M.; Rajabi, O.; Hadizadeh, F.; *Iran J. Basic Med. Sci.* **2023**, *26*, 37. [Crossref]
31. Uner, B.; Ozdemir, S.; Yildirim, E.; Yaba, A.; Tas, C.; Uner, M.; Ozsoy, Y.; *J. Drug. Delivery Sci. Technol.* **2023**, *81*, 104252. [Crossref]
32. Granados, P. A.; Gross, I. P.; Medeiros-Souza, P.; Sá-Barreto, L. L.; Gelfuso, G. M.; Gratieri, T.; Cunha-Filho, M.; *Pharmaceutics* **2025**, *17*, 586. [Crossref]
33. Ledeți, I.; Bengescu, C.; Cîrcioban, D.; Vlase, G.; Vlase, T.; Tomoroga, C.; Buda, V.; Ledeți, A.; Dragomirescu, A.; Murariu, M.; *J. Therm. Anal. Calorim.* **2020**, *141*, 1053. [Crossref]
34. Pharmaceutical Inspection Co-Operation Scheme (PIC/S); *Guide to Good Manufacturing Practice for Medicinal Products Part I*; PIC/S: Geneva, 2023. [Link] accessed in December 2025
35. Aucamp, M.; Milne, M.; *Eur. J. Pharm. Sci.* **2019**, *139*, 105057. [Crossref]
36. *The United States Pharmacopeia (USP)*, USP 22-NF 17, The United States Pharmacopeial Convention, Rockville, 1990.
37. *Matlab*, 9.14 (R2023a); The MathWorks Inc., USA, 2023.
38. Vyazovkin, S.; *J. Therm. Anal.* **1997**, *49*, 1493. [Crossref]
39. Koga, N.; Vyazovkin, S.; Burnham, A.; Favergeon, L.; Muravyev, N.; Pérez-Maqueda, L.; Sánchez-Jiménez, P.; *Thermochim. Acta* **2023**, *719*, 179384. [Crossref]
40. Órfão, J. J. M.; *AIChE J.* **2007**, *53*, 2905. [Crossref]
41. Aghili, A.; *Thermochim. Acta* **2021**, *705*, 179034. [Crossref]
42. Vyazovkin, S.; Burnham, A.; Criado, J.; Pérez-Maqueda, L.; Popescu, C.; Sbirrazzuoli, N.; *Thermochim. Acta* **2011**, *520*, 1. [Crossref]
43. Tikhonov, A. N.; Goncharskij, A.; *Ill -posed Problems in Natural Sciences*; Mir Publishers: Moscow, Russia, 1992.
44. Braga, J. P.; Lemes, N. H. T.; Borges, E.; Sebastião, R. C. O.; *Quim. Nova* **2016**, *39*, 886. [Crossref]
45. Spackman, P. R.; Turner, M. J.; McKinnon, J. J.; Wolff, S. K.; Grimwood, D. J.; Jayatilaka, D.; Spackman, M. A.; *J. Appl. Cryst.* **2021**, *54*, 1006. [Crossref]
46. Friedman, H. L.; *J. Polym. Sci.* **1964**, *6*, 183. [Crossref]
47. Venkatesh, M.; Ravi, P.; Tewari, S. P.; *J. Phys. Chem. A* **2013**, *117*, 10162. [Crossref]
48. Resentera, A. C.; Tancredi, N.; Plascencia, C. R.; *J. Therm. Anal. Calorim.* **2024**, *149*, 9389. [Crossref]
49. Vyazovkin, S.; Burnham, A. K.; Favergeon, L.; Koga, N.; Moukhina, E.; Pérez-Maqueda, L. A.; Sbirrazzuoli, N.; *Thermochim. Acta* **2020**, *689*, 178597. [Crossref]
50. Vyazovkin, S.; Achilias, D.; Fernandez-Francos, X.; Galukhin, A.; Sbirrazzuoli, N.; *Thermochim. Acta* **2022**, *714*, 179243. [Crossref]
51. Avrami, M.; *J. Chem. Phys.* **1939**, *7*, 1103. [Crossref]
52. Avrami, M.; *J. Chem. Phys.* **1940**, *8*, 212. [Crossref]
53. Avrami, M.; *J. Chem. Phys.* **1941**, *9*, 177. [Crossref]
54. Wittmann, A.; Wronski, T.; Shafirovich, E.; Schönnenbeck, C.; Brillard, A.; Brilhac, J. F.; Tschamber, V.; *Combust. Flame* **2025**, *272*, 113853. [Crossref]
55. Shirzad, K.; Viney, C.; *J. R. Soc. Interface* **2023**, *20*, 20230242. [Crossref]
56. Pérez-Cárdenas, F. C.; *Solids* **2022**, *3*, 447. [Crossref]
57. Kamel, L. T.; *Egypt. J. Appl. Sci.* **2019**, *34*, 194. [Crossref]
58. Fischer, O.; Lemaire, R.; Bensakhria, A.; *J. Therm. Anal. Calorim.* **2024**, *149*, 10941. [Crossref]
59. Yuan, X. M.; Xie, H. J.; Nie, D. P.; Zhang, Y.; Zhou, L.; Wu, Y. Y.; Wen, Z.; *RSC Adv.* **2023**, *13*, 16741. [Crossref]
60. Vyazovkin, S.; Sbirrazzuoli, N.; *Processes* **2023**, *11*, 1438. [Crossref]

Submitted: August 19, 2025
Final version online: December 17, 2025